

GAS-SOLID FLOW MODELING IN A COMBUSTION CHAMBER WITH MOVING BOUNDARY

Hazem El Sadek^{a,b}, XiaoBing Zhang^{a,b} and Mahmoud Rashad^{a,b}

^a Nanjing University of Science and Technology, School of Energy and Power Engineering,
zozaka2002@yahoo.com

^b Xiaolingwei, 200, Nanjing, Jiangsu Province, China

ABSTRACT

Numerical Simulation of the interior ballistic processes is a very difficult and challenging problem due to the existence of solid propellant and its products of combustion. Hence, modeling of the two phase flow is crucial to predict the interior ballistic parameters from the solid propellant ignition point till the projectile exit the gun muzzle. In this work, the computational fluid dynamics for two-phase flow of the interior ballistic process is presented. The numerical simulation is carried out by MacCormack's technique depending on the governing equations of the two-phase flow. A self-adapting method is used to expand the computational domain of the projectile motion and the moving control volume conservation method is utilized to adapt the moving boundary. This approach is applied to 76 mm naval medium caliber gun with guided projectile. The simulation results of the two-phase flow model with the projectile motion give a good agreement with the experimental results. The presented model enables successful solutions of many interior ballistic problems.

Keywords: interior ballistic, solid propellant, gas-solid flow, computational fluid dynamics, moving boundary

1. INTRODUCTION

Solid propellant is the most propellant in gun systems used to accelerate the projectile inside the bore. After ignition of the solid propellant, a large amount of energy is generated inside the combustion chamber of the gun. Hence, pressure and temperature of the products increase. Once the pressure reaches the starting pressure value, the projectile starts to move inside the barrel due to the expansion of the combustion products.

The simulation of the interior ballistic process for 76mm medium caliber naval gun was carried out before by using the Lumped Parameter Model [1]. The two-phase Flow simulation model will be better as it has more details for the interior ballistic performance with more accuracy, and it gives the chance to study the interaction process between the gas phase and the solid propellant phase.

In order to describe the interior ballistic performance, the two-phase flow simulation is required. The primary purpose of interior ballistic simulation is the prediction of projectile muzzle velocity and peak pressure inside the gun system. The two-phase flow model of interior ballistic process is very difficult to simulated, but it is a very challenge in the interior ballistic field. Due to many inter phase interaction between solid propellant and its products, and the complex chemical and physical phenomena that occurred in a very short time under high temperature and high pressure conditions.

At the initial time, the mixture of gas-propellant grains is placed in the combustion chamber and limited by breech at the left end, and by the projectile base at the right end. The scheme of that initial geometry is shown in Fig.1

In this work, the theoretical and numerical simulation of the two-phase flow is carried out in order to study the interior

ballistic phenomena. The simulation will be helpful to describe the physical and the chemical processes of the interior ballistic phenomena; in addition it will reduce the number of the experiments which is required for obtaining the optimal parameters for interior ballistic. The interior ballistic process was well demonstrated by some papers [2-6].

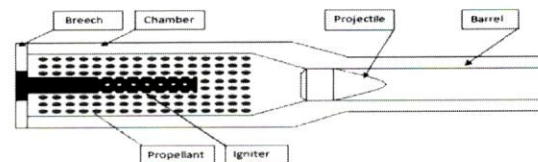


Fig.1. Gun system geometry with single propelling charge.

2. MATHEMATICAL MODEL

2.1 Governing Equations

The two-phase flow mathematical model is established to describe the physical and chemical process in the interior ballistic phenomena [7]. In this model; it is considered that gas phase and solid phase are continuum flows. The governing equations are made for the mass and momentum conservation laws for both phases (gas phase and solid phase), and the energy conservation for the gas phase. These equations are shown as follows:

The mass conservation equation of the gas phase:

$$\frac{\partial(\phi\rho_g A)}{\partial t} + \nabla \cdot (\phi\rho_g u_g A) = \dot{m}_c A + \sum \dot{m}_{ign} A \quad (1)$$

The mass conservation equation of the solid phase:

$$\frac{\partial[(1-\varphi)\rho_p A]}{\partial t} + \nabla \cdot [(1-\varphi)\rho_p u_p A] = -\dot{m}_c A \quad (2)$$

The momentum conservation equation of gas phase:

$$\frac{\partial(\varphi\rho_g u_g A)}{\partial t} + \nabla \cdot (\varphi\rho_g u_g u_g A) = -f_s A + \dot{m}_c u_p A + \sum \dot{m}_{ign} u_{ign} A - (\varphi A)\nabla p \quad (3)$$

The momentum conservation equation of solid phase:

$$\frac{\partial[(1-\varphi)\rho_p u_p A]}{\partial t} + \nabla \cdot [(1-\varphi)\rho_p u_p u_p A] + \nabla[(1-\varphi)R_p A] = f_s A - \dot{m}_c u_p A - (1-\varphi)A\nabla p \quad (4)$$

The energy conservation equation of the gas phase:

$$\begin{aligned} & \frac{\partial[\varphi\rho_g A(e_g + u_g \cdot u_g / 2)]}{\partial t} \\ & + \nabla \cdot [\varphi\rho_g u_g A(e_g + p/\rho_g + u_g \cdot u_g / 2)] \\ & = -Q_p A - f_s u_p A + \dot{m}_c A(e_p + p/\rho_p + u_p \cdot u_p / 2) \\ & + \sum \dot{m}_{ign} H_{ign} A - p \frac{\partial(A\varphi)}{\partial t} \end{aligned} \quad (5)$$

Where; φ is the volume fraction of the gas phase, u_g , u_p are the gas and solid velocity. ρ_g , ρ_p are the gas and the solid density. P , e_g are the pressure and internal energy of the gas phase. \dot{m}_c is the rate of gas mass generation due to propellant combustion. \dot{m}_{ign} is the mass flow rate of gas from vent holes of the igniter. H_{ign} is the stagnation enthalpy of the gas flow from vent holes. f_s , R_p and Q_p are interphase drag, intergranular stress, and interphase heat transfer respectively.

The above governing equations, Eqns. (1-5), for one-dimensional two-phase flow of a nonlinear hyperbolic partial differential equations, can be written in a vector form of conservation laws as:

$$\frac{\partial U}{\partial t} + \frac{\partial E}{\partial x} = S \quad (6)$$

Where, U , E , S are the conserved variables, the flux vector and the source vector respectively.

The components of U are the conserved variables:

$$U = \begin{pmatrix} U_1 \\ U_2 \\ U_3 \\ U_4 \\ U_5 \end{pmatrix} = \begin{pmatrix} \varphi\rho_g A \\ (1-\varphi)\rho_p A \\ \varphi\rho_g u_g A \\ (1-\varphi)\rho_p u_p A \\ \varphi\rho_g (e_g + u_g^2 / 2)A \end{pmatrix} \quad (7)$$

The components of E are the flux functions:

$$E = \begin{pmatrix} E_1 \\ E_2 \\ E_3 \\ E_4 \\ E_5 \end{pmatrix} = \begin{pmatrix} \varphi\rho_g u_g A \\ (1-\varphi)\rho_p u_p A \\ \varphi\rho_g u_g^2 A \\ (1-\varphi)(\rho_p u_p^2 + R_p)A \\ \varphi\rho_g u_g (e_g + u_g^2 / 2 + p / \rho_g)A \end{pmatrix} \quad (8)$$

And the components of S are the source term functions:

$$S = \begin{pmatrix} S_1 \\ S_2 \\ S_3 \\ S_4 \\ S_5 \end{pmatrix} = \begin{pmatrix} \dot{m}_c A + \sum \dot{m}_{ign} A + \dot{m}_k A \\ -\dot{m}_c A \\ -f_s A + \dot{m}_c u_p A + \sum \dot{m}_{ign} u_{ign} A + \dot{m}_k u_k A - (\varphi A)\nabla p \\ f_s A - \dot{m}_c u_p A - (1-\varphi)A\nabla p \\ (-Q_p A - f_s u_p A + \dot{m}_c A(e_p + p/\rho_p + u_p \cdot u_p / 2) \\ + \sum \dot{m}_{ign} H_{ign} A + \dot{m}_k H_k A - p \frac{\partial(A\varphi)}{\partial t}) \end{pmatrix} \quad (9)$$

2.2 Constitutive Relations

The two-phase flow simulation needs some constitutive relations to close the above governing equations. These relations describe the interaction between the gas phase and the solid phase such as Nobel-Abel equation of state, intergranular stresses, interphase drag force, and the interphase heat transfer.

- Nobel-Abel equation of state

The perfect gas equation of state is inappropriate in interior ballistic process. High temperature and high pressures require the real gas equation of state, such as Nobel-Abel Equation.

$$P(v - \beta) = RT \quad (10)$$

Where; P is the pressure, v is specific volume, β is gas co-volume, R is specific gas constant, and T is the temperature.

- Intergranular stresses

The intergranular stresses between the solid propellant particles can be calculated as follows:

$$R_p = \begin{cases} -\rho_{pc}^2 \frac{\varphi - \varphi_0}{1 - \varphi} \frac{\varphi}{\varphi_0} & \varphi \leq \varphi_0 \\ \frac{\rho_{pc}^2}{2k(1-\varphi)} [1 - e^{-2k(1-\varphi)}] & \varphi_0 < \varphi < \varphi^* \\ 0 & \varphi \geq \varphi^* \end{cases} \quad (11)$$

Where, φ_0 is the initial value of porosity, φ^* and c are calculated from Eqns. (12-13) respectively.

$$\varphi^* = \varphi_0 + 0.1513 \quad (12)$$

$$c = \begin{cases} c_1 \frac{\varphi_1}{\varphi} & \varphi \leq \varphi_0 \\ c_1 e^{-k(\varphi - \varphi_0)} & \varphi_0 < \varphi < \varphi^* \\ 0 & \varphi \geq \varphi^* \end{cases} \quad (13)$$

Where, c is the sound speed, k is factor of attenuation of intergranular stress.

- Interphase drag force

The interphase drag force can be calculated as follows:

$$f_s = \frac{1-\varphi}{d_p} |u_g - u_p| (u_g - u_p) \rho_g^* \xi \quad (14)$$

Where;

$$\xi = \begin{cases} 1.75 & \varphi \leq \varphi_0 \\ 1.75 \left(\frac{1-\varphi}{1-\varphi_0} \frac{\varphi_0}{\varphi} \right)^{0.45} & \varphi_0 < \varphi \leq \varphi_1 \\ 0.3 & \varphi > \varphi_1 \end{cases} \quad (15)$$

Where d_p is the equivalent diameter of the solid propellant, and φ_1 is calculated from the following relation:

$$\varphi_1 = \left[1 + 0.02 \frac{1-\varphi_0}{\varphi_0} \right]^{-1} \quad (16)$$

The theoretical and numerical modeling of the interior ballistic cycle for the used igniter is similar to the modeling of the two-phase flow in the gun chamber. The assumptions and full details of the igniter modeling are presented in [2].

3. NUMERICAL SOLUTION

3.1 Numerical Technique

The governing equations are discretised in a finite volume manner on a regular mesh with moving boundary to solve the Riemann problem. The solution of these equations is carried out by MacCormack's technique, it is an explicit finite difference method with second order accurate in both space and time. This technique consists of two steps; predictor step and corrector step.

-The predictor step is based on the right hand side with forward difference:

$$\bar{U}_i^{t+\Delta t} = U_i^t - \frac{\Delta t}{\Delta x} (E_{i+1}^t - E_i^t) + \Delta t S_i^t \quad (16)$$

-The Corrector step is based on the right hand side with rearward difference and substituting the predicted values of the time derivative $\bar{U}_i^{t+\Delta t}$ at time $(t + \Delta t)$:

$$U_i^{t+\Delta t} = \frac{1}{2} [U_i^t + \bar{U}_i^{t+\Delta t} - \frac{\Delta t}{\Delta x} (\bar{E}_i^{t+\Delta t} - \bar{E}_{i-1}^{t+\Delta t}) + \Delta t \bar{S}_i^{t+\Delta t}] \quad (17)$$

3.2 Numerical Verifications

The governing equation in Eq. (6) contains two Euler equations for gas phase and solid phase coupled with the source term. The numerical solution for the governing equations should be tested to verify the accuracy of the CFD code. In this work, Sod Shock Tube test is used [8]. This test consists of one dimensional Riemann problem with a computed domain $-1 \leq x \leq 1$. This solution is computed with 500 mesh cells, final time $t = 0.2$, and CFL = 0.9. The closed-form exact solution of the Riemann problem does not exist therefore an iterative scheme was carried out by Toro to obtain the exact solution of the Riemann problem [9].

The initial states of the Riemann problem are shown as:

$$\left. \begin{aligned} \rho(x, 0) &= \begin{cases} 1.0 & \text{for } x \leq 0 \\ 0.125 & \text{for } x > 0 \end{cases} \\ p(x, 0) &= \begin{cases} 1.0 & \text{for } x \leq 0 \\ 0.1 & \text{for } x > 0 \end{cases} \\ u(x, 0) &= \begin{cases} 0 & \text{for } x \leq 0 \\ 0 & \text{for } x > 0 \end{cases} \end{aligned} \right\} \quad (18)$$

Where, ρ is the density of the fluid, P is the pressure, and u is the fluid velocity.

The numerical solution of the Riemann problem using MacCormack's technique gives a good agreement with the exact solution of Sod Shock Tube test as illustrated in Figs.(2-4)

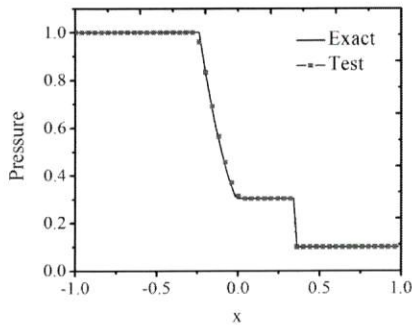


Fig.2 Numerical and exact solution of pressure through Sod tube test

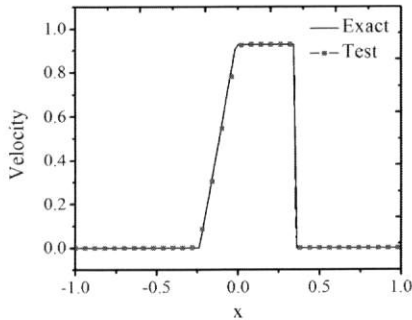


Fig.3 Numerical and exact solution of velocity through Sod tube test

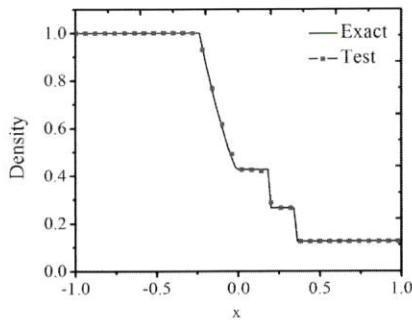


Fig.4 Numerical and exact solution of density through Sod tube test

3.3 Grid adaptation

In order to compute the position of the projectile base x_p that describe the extension of the last mesh cell behind the projectile base, we apply the fundamental principle of dynamics:

$$\frac{dv_p}{dt} = \frac{A_p P_p}{\varphi_1 m_p} \quad (19)$$

Where; v_p is the projectile velocity, A_p is the barrel cross-section, P_p is the pressure at the projectile base, φ_1 is coefficient of secondary energy losses, and m_p is the projectile mass.

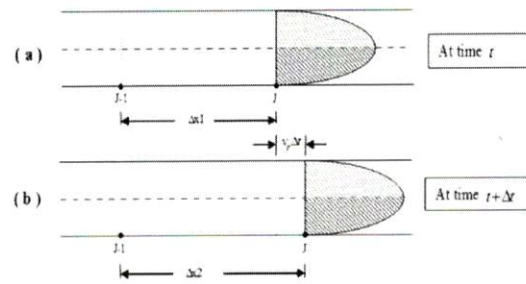


Fig.5. Schematic of grid adaption.

The computational domain has a fixed mesh cells with length Δx before moving of the projectile. Once the projectile start to move, the computational domain begins to change as the length of the last mesh cell begins to expand with length Δx_1 at time t . The grid adaption algorithm is carried out to solve this dynamic mesh problem. On the next iteration the time is denoted by $t+\Delta t$ and the length of the last mesh cell will be Δx_2 as shown in Fig.5.

The displacement of the projectile at the new time step $t+\Delta t$ will be calculated as follows:

$$\Delta x_2 = \Delta x_1 + v_p \Delta t \quad (20)$$

The length of the last mesh cell at the projectile base will increase every time step. The Self-Adaption algorithm is carried out to adapt this expansion and generate a new mesh cell according to the following conditions:

If $\Delta x_2 \leq 1.5\Delta x$, then:

The number of mesh cells will be the same, expand the length of the last cell Δx_1 to be Δx_2 .

If $\Delta x_2 > 1.5\Delta x$, then:

Add a new cell with length Δx , and of Δx_1 will take the value $\Delta x_2 - \Delta x$

3.4 Boundary Conditions

In this work, the reflective boundary conditions are used for both left and right ends of the computational domain before the projectile start to move. Once the projectile begins to move, the left end will be fixed and the reflective boundary condition is carried out, but the right end need to move behind the projectile. Hence, another suitable boundary condition method is required. The moving control volume conservation method is used to handle the motion of the right end at the projectile base [10-12].

4. RESULTS AND ANALYSIS

In this work, the two-phase flow code is carried out to 76 mm naval medium caliber gun, the detailed data of the used gun is illustrated as follows in Table 1.

4.1 Pressure Distribution

As shown in Fig.6, once the pressure at Vent-Holes inside the igniter reaches 20 MPa, the Vent-Holes ruptures and the flame jet flows from the igniter to the chamber penetrating the propellant at time 1.08 ms.

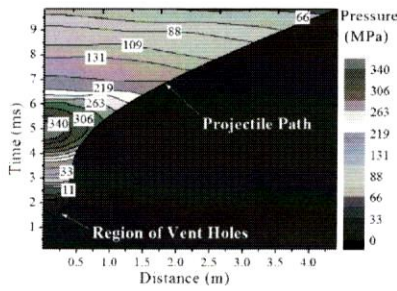


Fig.6. Pressure history on x-t diagram

The propellant starts the ignition at the broken Vent-Holes and the pressure will increase gradually inside the chamber. Once the pressure at the projectile base reaches 30 MPa, the projectile starts to move inside the bore, and the pressure continue in increasing till it reaches the maximum pressure inside the gun at time 5.4 ms, then the pressure decreases gradually until the projectile exit from the muzzle and the interior ballistic process ends.

Table 1. Data of 76 mm naval gun.

Parameter	Value	Unit
Gun Geometry		
Gun Caliber	0.076	m
Tube Length	4.045	m
Chamber Length	0.38	m
Projectile Mass	5.9	Kg
Chamber Volume	0.00354	m ³
Propellant (Double Base 7-Perforated)		
Mass	2.66	Kg
Impetus Force	980000	J/Kg
Ignition Temp.	615	K
Co-volume	0.001	m ³ /Kg
Density	1550	Kg/ m ³

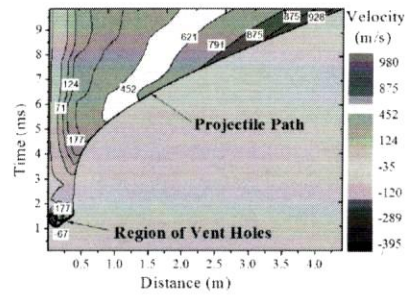
4.2 Velocity Profile

Figure 7, Shows the velocity profile for gas and solid phase in the interior ballistic process. Due to the jet flow from igniter to chamber through the Vent-Holes, the gas products will be formed. During the time from 1ms to 2ms some negative values for velocity are observed, as the gas products move towards the breech of the gun and the projectile base to allow the propellant ignition as shown in Fig.7a. After the projectile starts to move the gas velocity behind the projectile will take the value of projectile velocity, leaving the solid propellant behind it, thus it is observed that the values of solid velocity are less than the values of gas velocity as shown in Fig.7b.

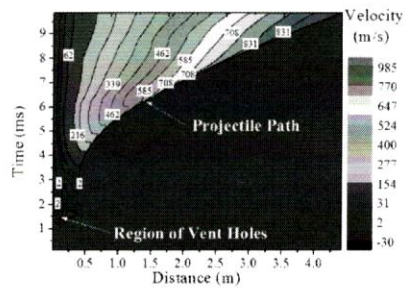
4.3 Gas Volume Fraction Profile

The gas volume fraction starts in the initial stage by its initial value calculated according to the propellant weight and the combustion chamber's volume. Once the Vent-Holes rupture, the gas volume fraction increases in the Vent-holes region as the releasing of the gas from igniter to chamber. Further, due to the left and right travelling waves of the flame, the propellant bed in the chamber starts to ignite by heat

transfer leading to decreasing of the propellant volume fraction and increasing of the gas volume fraction until the complete burning stage. At this stage, the gas volume fraction attains its maximum value as illustrated in Fig.8.



(a) Gas velocity.



(b) Solid velocity.

Fig.7. Velocity profile on x-t diagram.

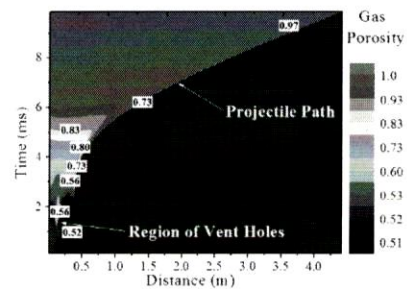


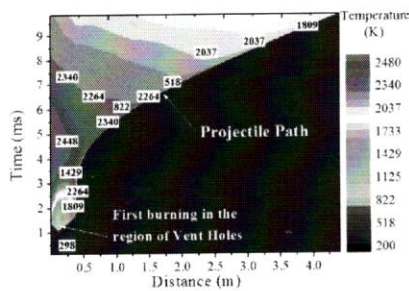
Fig.8. Gas volume fraction profile on x-t diagram.

4.4 Temperature profile

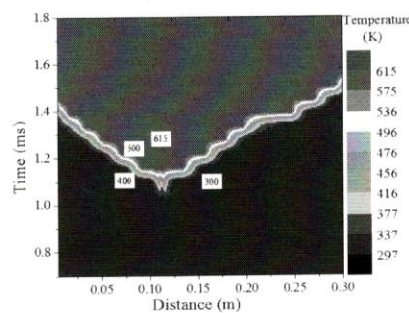
The temperature distribution of gas and solid phases are illustrated in Fig.9. At the initial phase of combustion, the gas temperature increases rapidly until it reaches the maximum value, 2450 K, at time 6.5ms. Then it starts to decrease gradually as the volume behind the projectile increase due to the projectile movement down the gun bore as shown in Fig.9a.

While, at the beginning of the ignition process of the main propellant charge around the igniter function the solid propellant particles near to the Vent-holes will firstly ignite, then the flame propagates in both sides of the gun chamber

causing the ignition of the whole propellant. The complete ignition takes place at about time 1.5 ms as shown in Fig. 9b. at that time the whole propellant is burned up and deliver all its energy to the projectile as a kinetic energy except some energy lost due heat transfer to the gun barrel.



(a) Gas temperature.



(b) Solid temperature.

Fig.9. Temperature distribution on x-t diagram.

5. VALIDATION OF THE SIMULATION RESULTS

The results from the interior ballistics experiment are limited, the velocity can be measured only at the muzzle, and the pressure can be measured at the breech, the comparison between the experimental and simulation results are shown in Table 2, this table shows an acceptance and agreement between the experimental and simulation results.

Table 2. Comparison between experimental and numerical results.

IB Parameter	Experimental results	Simulation results
Maximum chamber pressure [MPa]	345	342.8
Muzzle velocity [m/s]	983	987.75

6. CONCLUSIONS

The numerical simulation for the two-phase flow of the interior ballistic cycle is carried out for 76 mm naval medium caliber gun with guided projectile, the governing equations are discretised in a finite volume manner on a regular mesh with moving boundary, the moving control volume conservation method is used to handle the motion of the projectile inside the barrel, the Self-Adaption algorithm is used to adapt the expansion of the computational domain behind the projectile base. The solution is executed by MacCromack technique, this technique has been tested and validated to ensure that its accuracy and its ability to solve the governing equations of the two-phase flow model with moving boundary. The two-phase flow simulation gives a good agreement compared with the experimental results. The simulation will be helpful to achieve the required interior ballistic performance for the guided projectile by changing the interior ballistic parameters to increase the muzzle velocity and decrease the peak pressure which are required for the guided projectiles.

ACKNOWLEDGEMENTS

The research was supported by the Research Fund for the Natural Science Foundation of Jiangsu province (BK20131348), Key Laboratory Fund (Grant No. 9140C300103140C30001), People's Republic of China.

7. REFERENCES

1. H. Elsadek, X. B. Zhang and M. M. Rashad, Parametric study on mixed propellant for the medium caliber naval gun guided projectile, *Journal of engineering and Applied Science*, vol. 60, 1, pp.81-91, 2013.
2. Y. X. Yuan and X.B. Zhang, *Multiphase hydrokinetic foundation of high temperature and high pressure*, Publishing Company of Harbin Institute of Technology, Harbin, 2005.
3. N. C. Markator, Modeling of two-phase transient flow and combustion of granular propellants, *Int. J. Multiphase Flow*, vol. 12, 6, pp.913-933, 1986.
4. T. Sheu and S. M. Lee, Analysis of combustion processes in a gun interior ballistics, *International Journal of Computational Fluid Dynamics*, vol. 4, 1, pp. 57-71, 1995.
5. J. Nussbaum and P. Helluy, Numerical simulations of gas-particle flows with combustion, *Flow Turbulence and Combustion*, vol. 76, 4, pp.403-417, 2006.
6. H. Miura and A. Matsuo, Numerical prediction of interior ballistics performance of projectile accelerator by solid/gas two-phase reacting flow simulation, *48th AIAA Aerospace Sciences Meeting Including the New Horizons Forum and Aerospace Exposition*, vol. 48, 1, pp. 250-261, 2010.
7. Clarke and C. Lowe, CFD Modeling Of Solid Propellant Ignition, PhD. thesis, Cranfield University, Cranfield, 1996.
8. G. A. Sod, A survey of several finite difference methods for systems of nonlinear hyperbolic conservation laws,

- Journal of Computational Physics*, vol. 27, 1, pp. 1-31, 1978.
9. E. F. Toro, *Riemann Solvers and Numerical Methods for Fluid Dynamics*, Springer, 1997.
 10. S. G. Ahmed, A new algorithm for moving boundary problems subject to periodic boundary conditions, *International Journal of Numerical Methods for Heat & Fluid Flow*, Vol. 16, pp. 18-27, 2006.
 11. M. Faraji, H. El Qarnia, Numerical optimization of a thermal performance of a phase change material based heat sink., *International journal of heat and technology*, Vol.26,2, pp.17-24, 2008.
 12. J. M. Jalil, K. M. Abdel-Razak, Numerical and experimental investigation of optimum pipes spacing, *International journal of heat and technology*, Vol.27,2, pp.25-30, 2009.

